Journal of Catalysis 278 (2011) 297–309

Contents lists available at ScienceDirect

Journal of Catalysis

journal homepage: www.elsevier.com/locate/jcat

CO_2 methanation on Ru-doped ceria

Sudhanshu Sharma [b], Zhenpeng Hu [a], Peng Zhang [b], Eric W. McFarland [b], Horia Metiu [a,*]

[a] Department of Chemistry and Biochemistry, University of California, Santa Barbara, CA 93106, USA
[b] Department of Chemical Engineering, University of California, Santa Barbara, CA 93106, USA

ARTICLE INFO

Article history:
Received 21 September 2010
Revised 29 November 2010
Accepted 23 December 2010
Available online 3 February 2011

Keywords:
Ceria
Doped ceria
Methane
Carbon dioxide
Hydrogen
Methanation

ABSTRACT

We study the methanation of CO_2 catalyzed by ceria doped with Ni, Co, Pd, or Ru. $Ce_{0.96}Ru_{0.04}O_2$ and $Ce_{0.95}Ru_{0.05}O_2$ perform best, converting 55% of CO_2 with a 99% selectivity for methane, at a temperature of 450 °C. This is comparable to the best catalysts found previously for this reaction. $Ce_{0.95}Ru_{0.05}O_2$ was characterized by XRD, electron microscopy, BET, XPS, IR spectroscopy, and temperature-programmed reaction with Ar, H_2, CO, and $CO_2 + H_2$. Steady-state methanation was studied at several temperatures between 100 and 500 °C. We find that the methanation reaction takes place on the reduced $Ce_{0.95}Ru_{0.05}O_2$, and the role of the dopant is to make the reduction possible at lower temperature than on pure ceria. We discuss the potential for local and global effects of the dopant on catalytic chemistry.

1. Introduction

The conversion of CO_2 to methane ($CO_2 + 4H_2 \rightarrow CH_4 + 2H_2O$) transforms a molecule (hydrogen) that is difficult to store and transport into a molecule (methane) that is relatively easy to store and can be transported in millions of miles of existing natural-gas pipelines. Because most hydrogen today is produced from fossil hydrocarbons, its conversion to methane is not a sensible idea unless an inexpensive and renewable source of hydrogen is found (e.g. biomass or water). The hydrogenation of CO_2 is scientifically interesting for what it might teach us about activating CO_2, which is a topic of great current interest [1–40]. Sabatier and Senderens [41] seem to be the first to have produced methane from CO_2 and H_2, using Ni or Co catalysts.

In this article, we investigate CO_2 methanation by catalysts consisting of CeO_2 doped with Ni, or Co, or Pd, or Ru. Among these, the Ru-doped ceria is most active and selective, and therefore we have studied its properties in detail. The doped oxides are prepared by a combustion method, which has been used extensively in Hegde's group [42], and which tends to produce oxides in which the dopant atoms substitute the cations in the host oxide (in the case of Ru-doped CeO_2, we assume that Ru atoms substitute Ce atoms in CeO_2). In what follows we denote these catalysts by $Ce_{1-x}Ru_xO_2$.

It is difficult to provide a convincing proof that a doped oxide has been prepared and even more difficult to show that the Ru dopant is in the surface layer where it would influence most effectively the catalytic activity of the oxide. One way of increasing the confidence that a doped oxide has been prepared is to show that we have not prepared one of the possible alternatives: small metallic Ru clusters supported on ceria or small Ru oxide clusters supported on ceria.

It is conceivable that during the preparation by combustion and subsequent treatment, the Ru dopant segregates to form very small Ru metal clusters supported on the ceria. If this were the case, the Ru clusters would be visible in electron microscopy and the XPS spectrum would be that of metallic Ru, neither of which is observed. Furthermore, if Ru atoms segregate to make metal clusters, the catalytic chemistry of the system would be that of Ru supported on ceria, a system that has been extensively studied [27,29–34,36–40,43]. However, because the methanation activity of the metallic Ru depends on the support, on the method of preparation, and (possibly) on the size of the Ru clusters, we prepared our own Ru supported on ceria to have the same amount of Ru as the doped oxide prepared by combustion. We refer to this material as (5%Ru)CeO_2. We show that the catalytic activity of (5%Ru)CeO_2 is different from that of $Ce_{1-x}Ru_xO_2$, which indicates that the material we call $Ce_{1-x}Ru_xO_2$ does not consist of supported metallic Ru. In addition, if the presumed doped oxide consists of metallic Ru clusters, the IR spectrum of the surface exposed to CO would have absorption peaks typical of CO adsorbed on Ru, and we do not observe this.

* Corresponding author. Fax: +1 805 893 4120.
E-mail addresses: sudhanshu@engineering.ucsb.edu (S. Sharma), zhu@chem.ucsb.edu (Z. Hu), zhangpeng.pz@gmail.com (P. Zhang), mcfar@engineering.ucsb.edu (E.W. McFarland), metiu@chem.ucsb.edu (H. Metiu).

0021-9517/$ - see front matter © 2010 Elsevier Inc. All rights reserved.
doi:10.1016/j.jcat.2010.12.015

It is possible that during the preparation by the combustion method, the Ru atoms form *very small* clusters of ruthenium oxide supported on ceria. However, if the as-prepared catalyst consisted of ruthenium oxide clusters supported on ceria, then after some exposure to H_2 and CO_2, the RuO_2 cluster would be reduced and the catalytic activity of the material would be that of the supported Ru metal cluster. We do not observe such behavior.

Another argument supporting the assumption that we have prepared $Ce_{1-x}Ru_xO_2$ comes from the XRD measurements, which show that the material made by the combustion method has the fluorite structure of ceria, with a slight change in the lattice constant. This is a hallmark of a solid solution (i.e. substitutional doping).

All in all, the work presented here provides circumstantial evidence that the catalyst prepared by combustion is ceria doped with Ru. DFT calculations, together with the fact that ionic Ru is observed in the XPS spectrum, tell us that many of the Ru ions substitute Ce atoms in the surface layer or the layer below.

This article is organized as follows. Section 2 describes the preparation of the catalysts. The method used for the DFT calculations is explained in Section 3. Section 4 describes the catalytic activity, for CO_2 methanation, of $Ce_{1-x}Ru_xO_2$ and of (5%Ru)CeO_2. TPR measurements show that Ru-doped ceria has higher CO_2 conversion and higher selectivity to methane than ceria doped with Ni, or Co, or Pd, or than (5%Ru)CeO_2. Because of this, we dedicate the remainder of the article to the study of the $Ce_{0.95}Ru_{0.05}O_2$ catalyst. To determine its catalytic activity at steady state, we vary the temperature linearly to a certain value and maintain it until steady state is reached. Then, we perform another linear increase to a higher temperature and maintain it constant until steady state is reached, etc. We call this procedure the staircase temperature-programmed reaction (STPR). Section 5 presents results of TPR performed with $Ce_{0.95}Ru_{0.05}O_2$ exposed to Ar, H_2, or CO to determine the thermal stability of the doped oxide and its reducibility. Section 6 presents IR spectra of the catalyst surface during the reaction. These spectra show that $Ce_{0.95}Ru_{0.05}O_2$ is quickly contaminated by the trace CO_2 always present in Ar or H_2, which forms surface carbonates that are unstable at temperatures above 300 °C. We were unable to determine whether the hydroxyls and the carbonates are reaction intermediates or spectators. Section 7 shows that $Ce_{0.95}Ru_{0.05}O_2$ does not catalyze CO hydrogenation, which differentiates it from other methanation catalysts, which first reduce CO_2 to CO, and then undergo a Fischer–Tropsch conversion to hydrocarbons [8]. Section 8 summarizes our findings and discusses some of their implications. We suggest that the CO_2 methanation takes place on the reduced $Ce_{0.95}Ru_{0.05}O_2$ surface and that the role of the Ru dopant is to facilitate this reduction. We also speculate that a dopant can affect surface chemistry in two ways: locally, by modifying the chemical bonds of the oxygen atoms in the neighborhood of the dopant and globally, by changing the Fermi level of the system.

2. Catalyst preparation

The $Ce_{1-x}Ru_xO_2$ catalyst was synthesized by using the combustion method [42]. In a typical preparation, 2.5 g of ceric ammonium nitrate, 49.78 mg of $RuCl_3$, and 1.25 g of oxalic dihydrazide are dissolved in distilled water. The aqueous mixture is placed in a

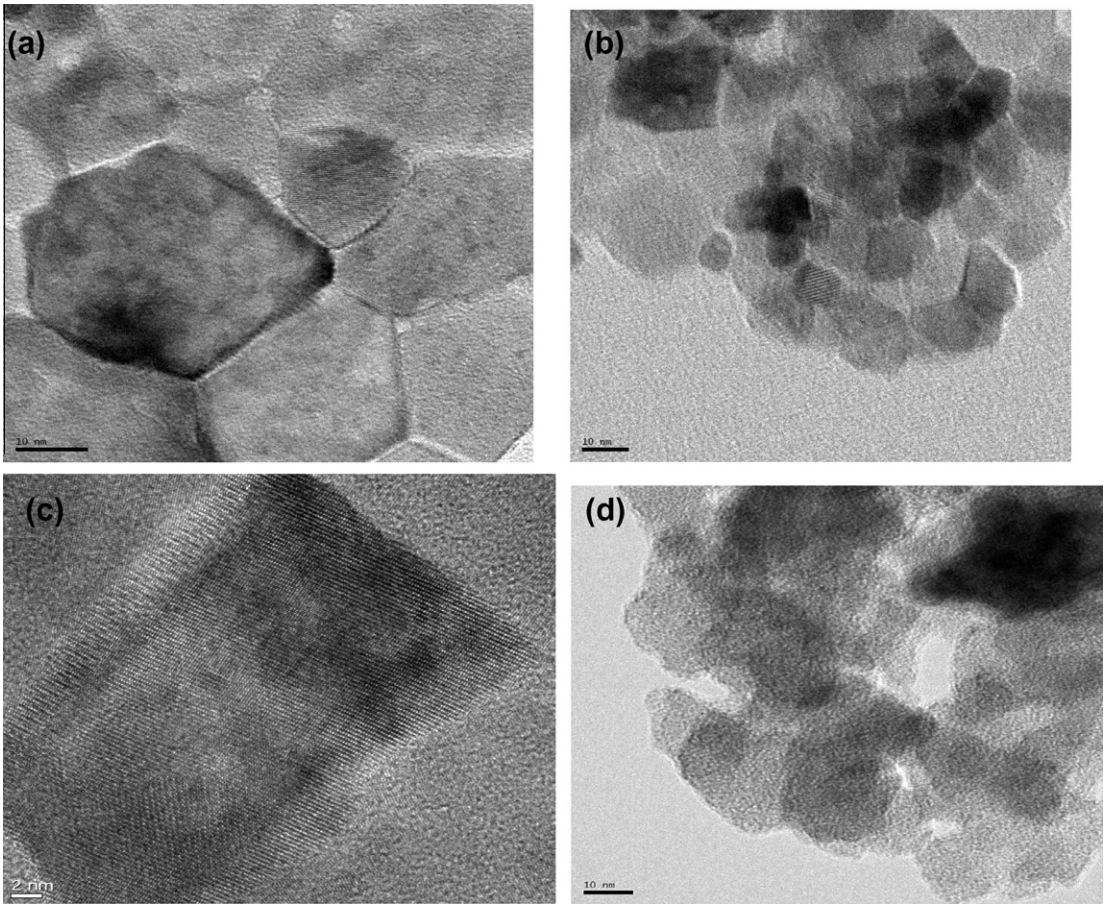

Fig. 1. Transmission electron microscopy (TEM) images of various ceria-based catalysts. (a and b) TEM of $Ce_{0.95}Ru_{0.05}O_2$ made by combustion, at different magnifications. (c) High-resolution TEM (HRTEM) of the same catalyst. (d) TEM image of 5%Ru dispersed over CeO_2 ((5%Ru)CeO_2) made by hydrazine reduction. The doped and the dispersed catalysts were calcined at 600 °C and 300 °C, respectively, overnight. Large crystallites represent ceria particles.

furnace and heated to 550 °C until combustion occurs spontaneously, giving the final $Ce_{0.95}Ru_{0.05}O_2$, product. The (5%Ru)CeO_2 catalyst was prepared by reducing an aqueous solution of $RuCl_3$ in contact with CeO_2 powder with hydrazine hydrate. To make 1.3 g of (5%Ru)CeO_2, 36.22 mg of $RuCl_3$ is dissolved in distilled water. CeO_2 powder is then mixed into this solution, to make slurry, to which we add slowly, drop by drop, a 40% hydrazine hydrate solution. This mixture is continuously stirred during the reduction. The product is repeatedly washed, first with water and then with alcohol. Finally, the catalyst is dried in a hot air oven for 10 h at 80 °C.

Ceria doped with Pd, Co, and Ni was also synthesized by the combustion method. For Pd-doped ceria, we used 2.5 g of ceric ammonium nitrate, 21.44 mg of palladium nitrate, and 1.25 g of oxalic dihydrazide (ODH). For Co-doped ceria, we used 2.5 gm of ceric ammonium nitrate, 60 mg of cobalt acetate, and 1.2 g of ODH. For Ni-doped CeO_2, we used 2.5 g of ceric ammonium nitrate, 60 mg of nickel acetate, and 1.34 g urea. These compounds were dissolved in distilled water and were combusted at 500 °C to give the doped oxides.

3. Computational method

It is believed that the standard generalized gradient approximation (GGA) of the density functional theory (DFT) makes errors when used to describe ceria [44–47] and that the results are improved by using the GGA + U method [48]. As yet it is not clear how accurate this method is for calculating binding energies or activation energies. Nevertheless, at this time, this seems to be the best option available, when one needs to study systems having a large number of electrons. Because we are interested in getting good values for the total energy, we use $U - J = 5.5$ eV since this reproduces the energy of the reaction $Ce_2O_3 + \frac{1}{2}O_2 \rightarrow 2CeO_2$ and gives accurate values for the lattice parameters of both oxides [47,49]. The LDA + U results are closer to experiments than those obtained with PW91 + U, and the LDA calculations are more efficient. For this reason, we use spin-polarized LDA + U with the implementation provided by the VASP program [50–53], with PAW pseudopotentials having the electron configurations $[Kr4d]5s^25p^64f^15d^16s^2$, $[Kr]4d^75s^1$, $[He]2s^22p^4$, and $[He]2s^22p^2$ for Ce, Ru, O, and C atoms, respectively. We used a slab having three CeO_2 layers (9 atomic layers) with a 3×3 surface supercell shown in Section 7. The supercell has a size of $11.45 \times (11.45 \times \sqrt{3}/2) \times 22.79$ Å^3, contains 82 atoms, and has a vacuum layer of 15 Å. The Ru dopant replaces a Ce atom in the outermost layer of the CeO_2(1 1 1) surface. A Gamma centered $2 \times 2 \times 1$ k-point mesh and a plane-wave basis set having a 400 eV energy cutoff were used in all calculations.

During the optimization of the geometry, the oxygen atoms in the bottom layer were held fixed at the positions they would have in the bulk; the atoms in the other eight atomic layers were allowed to relax until the force on each atom was less than 0.02 eV/Å, and the energy difference between two self-consistent steps was less than 10^{-4} eV. The energy optimization was stopped when the energy difference between two self-consistent steps was 10^{-5} eV.

4. Physical characterization

4.1. Electron microscopy

Images of the catalyst (Fig. 1) were obtained by Transmission Electron Microscopy (TEM; FEI-Technai G2 Sphera Microscope with a field emission gun 200 kV, point resolution 0.24 nm; line resolution 0.14 nm) and by high-resolution Transmission Electron Microscopy (HRTEM; FEI Titan 300 kV FEG TEM/STEM, point resolution 0.2 nm). They show characteristic lattice fringes that indicate that $Ce_{0.95}Ru_{0.05}O_2$ is crystalline. Dark regions are also present (especially in Fig. 1b), which might indicate a phase separation of Ru or RuO_2. However, the abundance of the dark region greatly exceeds what one would expect from the 5% Ru used in the preparation. Analysis of the HRTEM image in Fig. 1c indicates continuous lattice fringes with no evidence of separate phases. The TEM image of (5% Ru)CeO_2 (Fig. 1d) shows different morphology than that of $Ce_{0.95}Ru_{0.05}O_2$, further evidence that the doped oxide catalyst is different from the dispersed one.

4.2. X-ray diffraction (XRD)

The XRD powder diffraction patterns were obtained between 10° and 80° (Philips XPERT MPD, Cu Kα). Gold powder was used as the internal standard for determining the peak shifts when the oxide is doped.

Both the CeO_2 and $Ce_{0.95}Ru_{0.05}O_2$ crystallize in the fluorite structure (Fig. 2a and b, respectively). The XRD patterns in the region between 25° and 42° show no evidence of Ru metal or RuO_2 in $Ce_{0.95}Ru_{0.05}O_2$. This is consistent with the TEM images. Fig. 2c shows the XRD spectrum of (5%Ru)CeO_2.

Further support for the fact that $Ce_{0.95}Ru_{0.05}O_2$ is a solid solution of Ru in ceria is the shift in the XRD peak position for $Ce_{0.95}Ru_{0.05}O_2$ compared to that for the undoped CeO_2 (Fig. 2d). The lattice parameters, calculated with the Bragg equation, are 5.3826 Å and 5.3864 Å (for CeO_2 and $Ce_{0.95}Ru_{0.05}O_2$, respectively); the lattice parameter increases upon doping with Ru. The ionic radii of Ru(III)

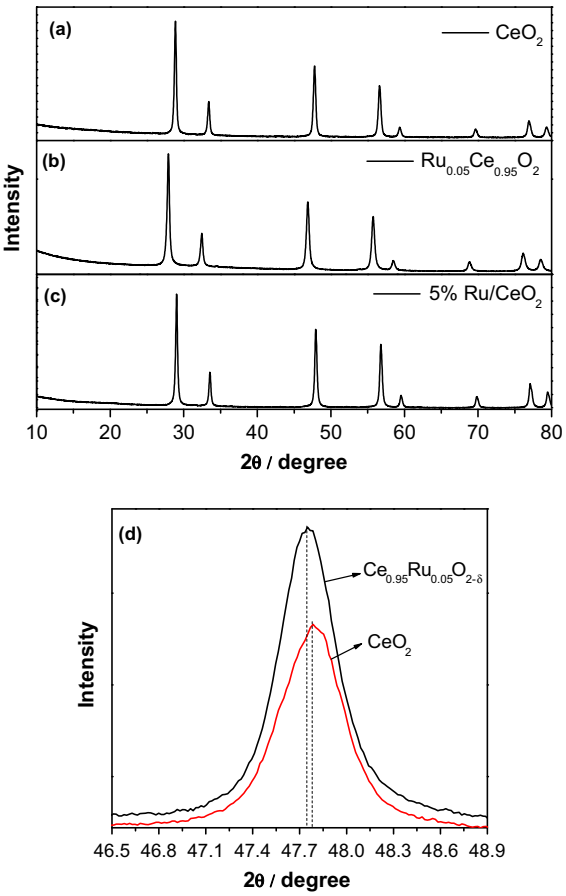

Fig. 2. X-ray diffraction (XRD) patterns for various ceria-based catalysts: (a) CeO_2; (b) $Ce_{0.95}Ru_{0.05}O_2$; (c) (5%Ru)CeO_2. (d) The XRD peaks of $Ce_{0.95}Ru_{0.05}O_2$ and CeO_2 and the peak shift.

and Ru(IV), in a 6-coordinated octahedral environment, are 82.0 and 76.0 Å, respectively. The ionic radii of Ce(III) and Ce(IV), in an 8-coordinated site, are 128.3 and 111.0 Å, respectively. Based on the ion size alone, one would expect that the ceria lattice would shrink when Ru substitutes Ce. This is not the case here. In previous work [54], it was assumed that the increase in the lattice constant is caused by the reduction of Ce^{4+} to Ce^{3+} when ceria is doped with Ru. The fact that a change of the lattice parameters is observed indicates that a substantial fraction of the Ru dopants must be located in the bulk.

The XRD results of $Ce_{0.98}Pd_{0.02}O_2$, $Ce_{0.95}Co_{0.05}O_2$, and $Ce_{0.95}Ni_{0.05}O_2$ are shown in Fig. 3. They all crystallize in the fluorite structure. No metal dopant or dopant-oxide peaks are seen in the XRD range between 25 and 50, which suggests that doped oxides have formed.

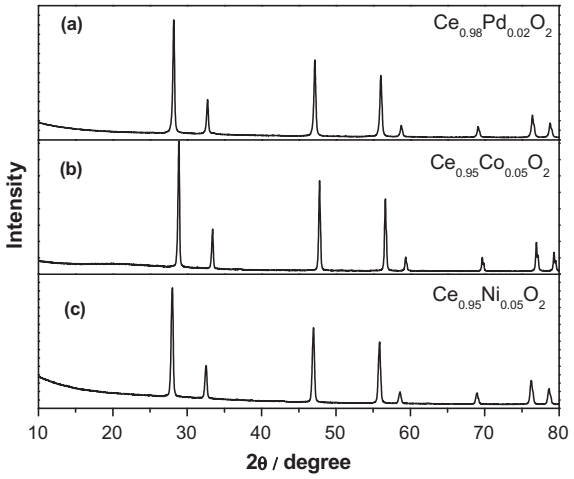

Fig. 3. The XRD patterns of (a) $Ce_{0.98}Pd_{0.02}O_2$, (b) $Ce_{0.95}Co_{0.05}O_2$ and (c) $Ce_{0.95}Ni_{0.05}O_2$.

4.3. Surface area

The Brunauer–Emmett–Teller (BET) measurements performed at liquid N_2 temperature (Micromeritics Tristar 3000 system) give a surface area of 16.19 m^2/g for $Ce_{0.95}Ru_{0.05}O_2$ and 13.2 m^2/gm for (5%Ru)CeO_2. This allows us to estimate the number of Ce atoms in the surface layer per gram of material. If we assume that all Ru atoms introduced with the precursor will be in the surface layer, they will have to replace all Ce atoms on the surface. This is very unlikely and therefore some of the Ru must be located in the bulk. This is consistent with the XRD results that indicate that doping causes a change in the lattice parameters of the fluoride structure.

4.4. X-ray photoelectron spectroscopy (XPS)

The XPS spectra were obtained with Al Kα radiation (Kratos Axis Ultra X-ray Photoelectron Spectroscopy), and the binding energies were corrected using C(1s) at 285.0 eV. The spectrometer has a resolution of 0.6 eV.

The Ru(3p) core level spectrum of the as-prepared $Ce_{0.95}Ru_{0.05}O_2$ is shown in Fig. 4a. The Ru($3p_{3/2}$) binding energy is 463.1 eV (the Ru(3p) region is examined because Ru($3d_{5/2,3/2}$) states overlap with C(1s)). The binding energy of Ru($3p_{3/2}$) in RuO_2 is[54] 462.7 eV, which differs by 0.4 eV from the binding energy of Ru($3p_{3/2}$) in $Ce_{0.95}Ru_{0.05}O_2$. This difference is probably due to a difference in the environment: the Ru oxygen distance and the location of the oxygen atoms in $Ce_{0.95}Ru_{0.05}O_2$ are different from those in RuO_2. If we must assign a formal charge to the Ru dopant, we opt for +4 because Ru oxides with higher formal charge are unstable [55,56]. The XPS spectrum of the catalyst after the reaction is shown in Fig. 14b. No change in the Ru($3p_{3/2}$) binding energy is observed, when compared to the as-prepared catalyst. This indicates that the state of the ionic Ru in the surface region does not change when the methanation reaction is performed. This is consistent with the fact that the catalytic performance is constant for 900 min.

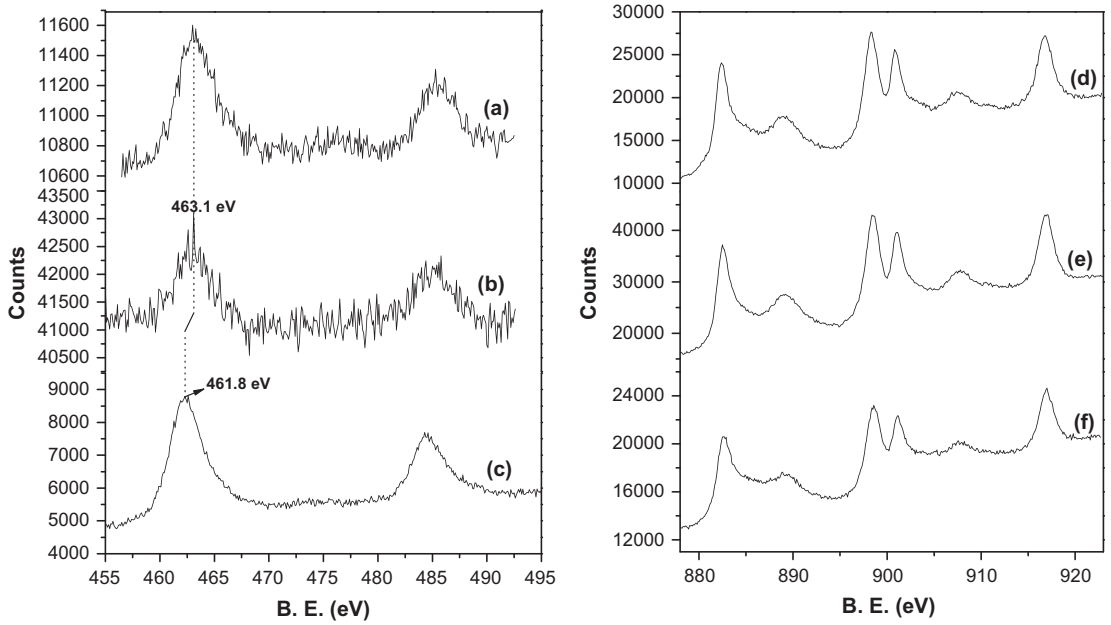

Fig. 4. X-ray photo electron spectra (XPS) of various CeO_2 catalysts. XPS of Ru(3p) core level in $Ce_{0.95}Ru_{0.05}O_2$: (a) before the reaction (as-prepared catalyst) and (b) after the methanation reaction in the flow of 5 ml/min for argon, 2 ml/min for CO_2, and 8 ml/min for H_2 (used catalyst). (c) XPS of Ru(3p) in (5%Ru)CeO_2 made by hydrazine reduction. XPS of Ce(3d) core level in $Ce_{0.95}Ru_{0.05}O_2$, (d) as-prepared catalyst and (e) after the methanation reaction in the flow of 5 ml/min for argon, 2 ml/min for CO_2, and 8 ml/min for H_2 (used catalyst). (f) XPS of Ce(3d) in (5%Ru)CeO_2. The binding energies are corrected by using carbon as the reference. The as-prepared doped and the dispersed catalysts were calcined at 600 °C and 300 °C, respectively, overnight.

The Ru(3p) core level spectrum of (5%Ru)CeO_2 (Fig. 4c) shows Ru($3p_{3/2}$) binding energy at 461.8 eV, consistent with the presence of Ru metal in the impregnated catalyst [54,57,58].

Since XPS measurements are sensitive to atoms in the surface region, some of the Ru atoms must be located near the surface, while the XRD results suggest that some are in the bulk. To estimate how much Ru is in the surface layer, we have measured the Ru(3p) spectrum in a sample consisting of CeO_2 mixed with RuO_2 in the same proportion as in $Ce_{0.95}Ru_{0.05}O_2$. By comparing the areas under the peaks in these two spectra, we estimate that three out of five Ru atoms are in the surface region of $Ce_{0.95}Ru_{0.05}O_2$.

Calculations of the energy of a CeO_2(1 1 1) slab with the Ru dopant in different locations give the following results: the energy when the dopant is in the second Ce layer is smaller by 0.28 eV than when the dopant is in the top layer. If the distribution of the Ru atoms reaches thermodynamic equilibrium, they will prefer to sit in the second Ce layer. The fact that there are Ru atoms in the surface region and in the bulk indicates that the mobility of the Ru atoms, during the synthesis of the doped ceria, is not high enough for these atoms to reach the equilibrium distribution. In addition, we note that given the area of the catalyst and the number of the Ru atoms used in synthesis, it is not possible for all Ru atoms to be in the subsurface layer.

The XPS spectrum of Ce(3d), of the as-prepared $Ce_{0.95}Ru_{0.05}O_2$ (Fig. 4d), of the catalyst after the methanation reaction (Fig. 4e), and of (5%Ru)CeO_2 (Fig. 4f) show that Ce is primarily present in the +4 oxidation state. The peak at 882.7 eV, along with its satellite peaks (6.4 and 16.0 eV below the main peak), is characteristic of [59] Ce^{4+} in CeO_2. The peak of Ce^{3+}(3d), in Ce_2O_3, is that of Ce($3d_{5/2}$), at 883.3 eV, along with an intense satellite [59] at 887.1 eV. Comparing the XPS spectra in Fig. 4d–f, with the deconvoluted spectra [60] of CeO_2, suggests that 10–15% of the Ce atoms in the surface region are Ce^{3+} and the remainder are Ce^{4+}. Most likely Ce^{3+} is formed because of oxygen vacancies in the material.

5. The methanation reaction

The activity of the catalysts was measured in a packed bed reactor, which is a 6-mm-diameter glass tube, 300 mm in length, fitted inside a stainless steel heating block. Twenty milligrams of catalyst was placed inside the tube with quartz wool at both ends. The geometric volume was 0.088 cm^3, and the void fraction was approximately 82%. Argon was the carrier gas and the calibration standard. The volumetric flow rates of argon, carbon monoxide, and oxygen were controlled by mass flow controllers (MKS). Typical experimental flow rates were 5 ml/min for argon, 2 ml/min for CO_2, and 8 ml/min for H_2, which gave an approximate space time of 0.35 s. The product gas was sampled directly at the reactor outlet with a differentially pumped mass spectrometer (Stanford Research Systems) through a controlled leak valve. For temperature-programmed reaction (TPR) studies, the temperature was ramped at the rate of 10 °C min^{-1} using a programmable temperature controller (Omega, CSC32). Before performing TPR, the catalyst was pretreated in Ar, at 500 °C, for 1 h, to degas it.

The TPR results for the methanation of CO_2 by H_2, catalyzed by $Ce_{0.98}Co_{0.02}O_2$, $Ce_{0.95}Pd_{0.05}O_2$, $Ce_{0.95}Ni_{0.05}O_2$, or $Ce_{0.95}Ru_{0.05}O_2$, are shown in Fig. 5. $Ce_{0.95}Pd_{0.05}O_2$ catalyzes the reverse water–gas shift (RWGS) reaction ($CO_2 + H_2 \rightarrow CO + H_2O$) and produces no methane in the temperature range 100–500 °C. $Ce_{0.95}Co_{0.05}O_2$ and $Ce_{0.95}Ni_{0.05}O_2$ catalyze methanation with low selectivity, since this reaction competes with the RWGS reaction. Clearly $Ce_{0.95}Ru_{0.05}O_2$ has the best performance: it starts producing methane at ~270 °C, reaches the highest methane yields at ~480 °C, with 55% CO_2 conversion and 99% selectivity for methane. The conversion and the selectivity of all doped oxides we have studied are given in Table 1.

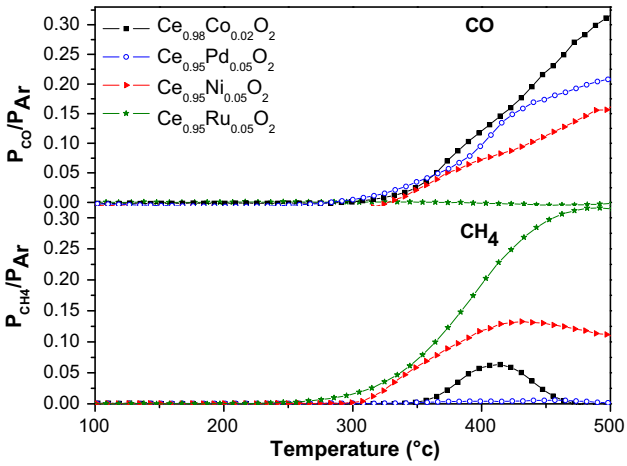

Fig. 5. Temperature-programmed reaction (TPR) of CO_2 methanation by H_2 on different doped-ceria catalysts. The graph gives the partial pressures of CO and CH_4 at the outlet of the reactor, normalized to the Ar pressure. The flow of the gases was 5 ml/min for argon, 2 ml/min for CO_2, and 8 ml/min for H_2. $Ce_{0.95}Ru_{0.05}O_2$ catalyst shows the highest activity with the lowest reaction-onset temperature.

Pure ceria, prepared by the combustion method, is inert in this temperature range. This may happen because of the high temperature reached during preparation [61,62] which has been shown to make CeO_2 inactive as an oxygen reservoir.

The TPR results for the methanation reaction on (5%Ru)CeO_2 are shown in Fig. 6. This catalyst is clearly different from the doped oxide. Comparing Fig. 5 to Fig. 6, we see that the activity for methanation of the (5%Ru)CeO_2 catalyst is inferior to that of $Ce_{0.95}Ru_{0.05}O_2$. While the production of CH_4 on $Ce_{0.95}Ru_{0.05}O_2$ grows monotonically with temperature, on (5%Ru)CeO_2 it reaches a maximum around 425 °C and then decreases. The total CO_2 conversion over the doped oxide is 55% and over the impregnated oxide is 25%. The methane selectivity of (5%Ru)CeO_2 is 99% at 375 °C, and it drops to almost 5% when the temperature is increased to 450 °C. On the other hand, the doped catalyst shows 99% selectivity at both temperatures.

We studied (5%Ru)CeO_2 only to prove that the material made by the combustion method is not metallic Ru supported on ceria. The reader interested in CO_2 hydrogenation by supported Ru can find extensive information in the literature [27,29–34,36–40,43]. From now on, we focus on $Ce_{0.95}Ru_{0.05}O_2$.

The steady-state activity of the $Ce_{0.95}Ru_{0.05}O_2$ catalyst was investigated by varying the temperature linearly in time, as in TPR, until the temperature of interest is reached. Then, the temperature is held constant until the methanation reaction reaches steady state. Next, the temperature is again increased linearly until the next temperature is reached, where it is again held constant until

Table 1
The methanation activity of $Ce_{1-x}M_xO_2$ (M = Ru, Co, Ni, Pd). CO_2 conversion is calculated at the temperature specified in the second column. Gas composition: 5 ml/min for Ar, 2 ml/min for CO_2, 8 ml/min for H_2.

Catalyst	Temperature (°C)	CO_2 conversion (%)	Maximum CH_4 selectivity (%)
$Ce_{0.99}Ru_{0.01}O_2$	500	16	90
$Ce_{0.98}Ru_{0.02}O_2$	500	24	95
$Ce_{0.97}Ru_{0.03}O_2$	480	51	99
$Ce_{0.96}Ru_{0.04}O_2$	450	55	99
$Ce_{0.95}Ru_{0.05}O_2$	450	55	99
$Ce_{0.95}Co_{0.05}O_2$	500	49	0
$Ce_{0.95}Ni_{0.05}O_2$	500	50	52
$Ce_{0.98}Pd_{0.02}O_2$	500	50	0

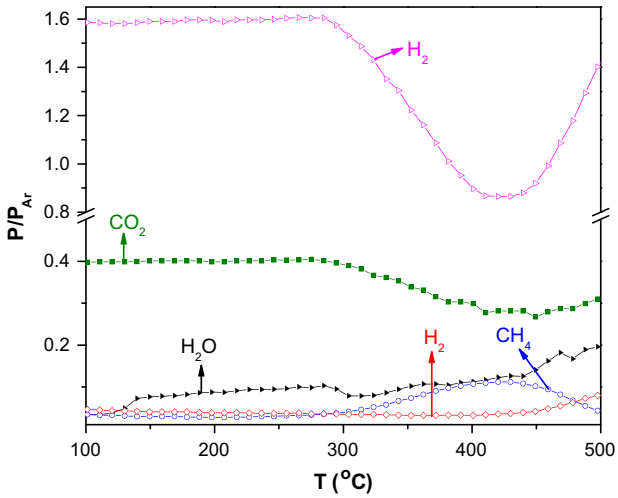

Fig. 6. Temperature-programmed reaction (TPR) of CO_2 methanation by H_2 over 5% Ru dispersed over CeO_2 ((5%Ru)CeO_2) catalysts made by hydrazine reduction. The flow rates are 5 ml/min of argon, 2 ml/min of CO_2, and 8 ml/min of H_2. The partial pressures are normalized by the pressure of Ar. The catalyst was pretreated in a flow of Ar, at 500 °C for an hour.

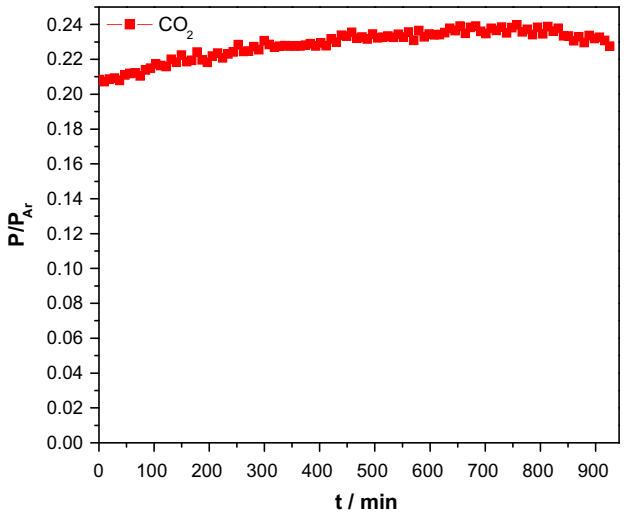

Fig. 8. Temperature-programmed reaction (TPR) for CO_2 methanation by H_2 over the $Ce_{0.95}Ru_{0.05}O_2$ catalyst made by combustion. We show the partial pressure of CO_2 after the reaction, normalized by the Ar pressure. The flow rates were 5 ml/min of argon, 2 ml/min of CO_2, and 8 ml/min of H_2, and the temperature was 325 °C. The catalyst was pretreated in the flow of Ar at 500 °C for an hour.

the system reaches the steady state, etc. This is TPR with a "staircase" temperature variation instead of a linear one. We call this a steady-state TPR (STPR). The results of one such measurement are shown in Fig. 7. The black curve (solid curve in the black and white figure) shows the temperature (the temperature scale is on the right-hand axis). We determine the steady states for temperatures between 300 °C and 500 °C, varied with increments of 50 °C. Methane production starts slightly below 300 °C and reaches a maximum at 400 °C. No CO is formed up to this temperature. A small amount of CO is seen at 450 °C and more is formed at 500 °C. CO production takes place with no change in CO_2 output, but with a loss of methane. This suggests that CO is produced by steam reforming of the methane produced by the reaction.

Upon reaching 500 °C, we step the temperature back to 450 °C and the reaction proceeds as it did when we increase the temperature from 400 °C to 450 °C; the state of the catalyst is reversible.

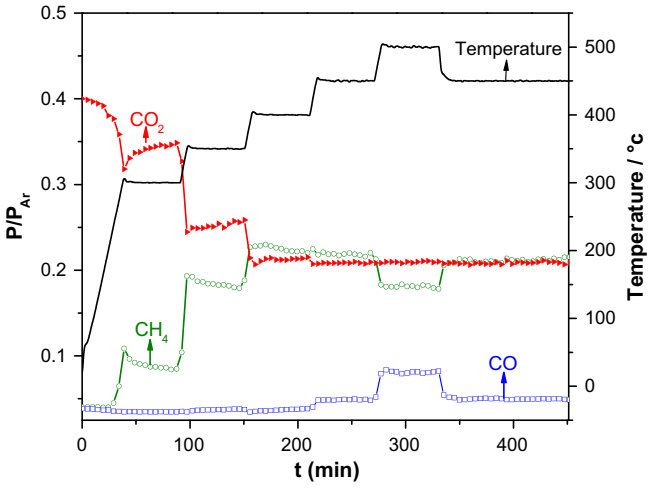

Fig. 7. Staircase temperature-programmed reaction (STPR) over $Ce_{0.95}Ru_{0.05}O_2$ catalyst made by combustion. Flow rates are 5 ml/min of argon, 2 ml/min of CO_2, and 8 ml/min of H_2. The temperature was held constant for almost 40 min to reach steady state. Partial pressures are normalized by the partial pressure of Ar. The catalyst was pretreated in a flow of Ar at 500 °C, for an hour. A change in the reaction behavior is noticed above 450 °C.

Running the reaction on $Ce_{0.95}Ru_{0.05}O_2$ for over 16 h, at 325 °C, shows no decrease in CO_2 conversion (Fig. 8). Direct observation of the catalyst showed no sign of darkening, which indicates that coking or the bulk reduction of the catalyst is not significant. We also maintained the reaction at 450 °C for 40 min and found no change in performance.

The results presented in Table 1 show that CO_2 conversion by $Ce_{1-x}Ru_xO_2$ increases with x; high conversion and selectivity are reached for $x > 0.03$. Since Ru is expensive, having an active catalyst with such a low Ru loading is advantageous.

6. Chemical characterization of the catalyst

The chemical properties of the $Ce_{0.95}Ru_{0.05}O_2$ were studied by performing temperature-programmed reduction (TPR) with H_2 and CO, and temperature-programmed desorption (TPD) experiments in which we heated $Ce_{0.95}Ru_{0.05}O_2$ and monitored O_2 emission, water formation from surface hydroxyls and CO_2 formation by the decomposition of surface carbonate.

In Fig. 9, we show the gases formed upon heating $Ce_{0.95}Ru_{0.05}O_2$ in a TPD experiment. Determining water evolution is difficult because of the presence of the background water. The water signal is strong at room temperature, and it is constant up to ~150 °C. After this temperature, the amount of water escaping from the reactor decreases monotonically up to 600 °C. There is no change in the signal that would allow us to distinguish water that was molecularly adsorbed from water formed from the hydroxyls on the surface. Between ~200 °C and 350 °C we observe CO_2, which is produced by the decomposition of surface carbonates. The IR experiments described later show that carbonates are formed readily even with trace contamination of Ar with CO_2. We do not see any oxygen desorption at temperatures below 600 °C. TPD experiments have been carried out on pure ceria [63–67], and the results depend strongly on the method of preparation and the degree of dispersion of the oxide. In some cases, no O_2 desorption has been observed [68] upon heating to 1100 °C. For high-area ceria particles (~12 nm across), oxygen desorption can take place [64] at a temperature as low as ~350 °C. The strong dependence of these results on the method of preparation makes it difficult to compare our TPD results on $Ce_{0.95}Ru_{0.05}O_2$ with the literature

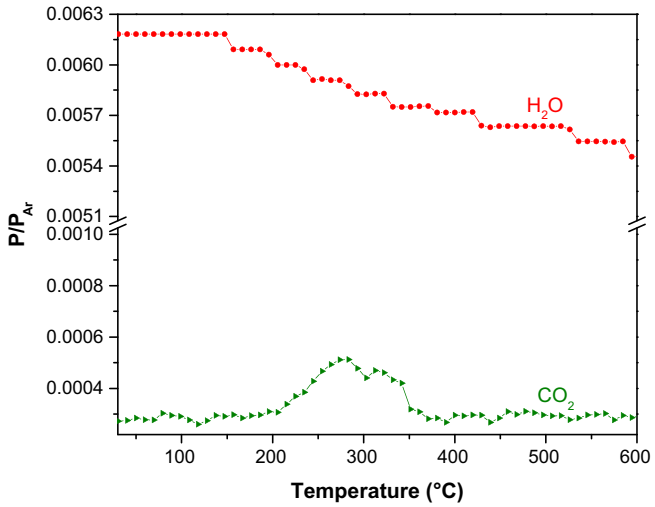

Fig. 9. Temperature-programmed desorption (TPD) of as-prepared $Ce_{0.95}Ru_{0.05}O_2$ catalyst made by combustion. Heating is performed in a flow of Ar (15 cc/min). The partial pressures are normalized by the partial pressure of Ar. CO_2 production indicates carbonate decomposition.

results on ceria. In addition, it is possible that the samples studied in the literature have low levels of dopants, which may make their behavior different from that of pure ceria.

The results of temperature-programmed reduction experiments of $Ce_{0.95}Ru_{0.05}O_2$ with H_2 are shown in Fig. 10. Before performing this reaction, the catalyst was heated in the flow of Ar at 500 °C for an hour to remove the adsorbed water, the residual water in the reactor, and the carbonates from the surface. At a temperature below ~130 °C, we observe background water and, perhaps, water produced by desorption from the surface (compare to Fig. 9), but no hydrogen consumption. The H_2 signal starts decreasing as the temperature exceeds ~130 °C, and this is accompanied by an increase in water signal. The amount of hydrogen exiting the reactor reaches a minimum at ~200 °C, and the amount of water produced is maximum at the same temperature. Above ~200 °C, the amount of H_2 that manages to pass through the reactor increases monotonically with the temperature and the amount of water decreases. This happens because by the time the sample reached ~200 °C, the surface is already reduced and this makes it more difficult for H_2 to remove oxygen from the surface. Depending on the partial pressure of the hydrogen, it is possible that the reduction will go on, if the temperature is sufficiently high, until all oxide is reduced to metallic Ce and Ru. In our experiments, the sample is exposed to H_2 for a short time and it is likely that the water is produced only by the reaction with the oxygen atoms in the surface layer.

This experiment tells us that the reduction of $Ce_{0.95}Ru_{0.05}O_2$ by H_2 takes place at a lower temperature than the methanation of CO_2, and therefore the methanation catalyst is the reduced $Ce_{0.95}Ru_{0.05}O_2$ surface.

The experiments on the reduction of pure ceria [68–72] by H_2 show a marked dependence on the method of preparation, the hydrogen pressure, the method of measurement, the presence or absence of carbonates and hydroxyls on the surface, and perhaps on unintentional doping by impurities in the precursors. In general, the reduction starts at lower temperature on samples having a larger surface area per gram. Presumably this happens because at large surface area enough water molecules are produced by the reduction of the surface layer to be detected. Given all these complications, it is difficult to choose a unique value for the lowest temperature at which H_2 consumption by pure ceria takes place. Perrichon et al. [69] found an onset temperature of 347 °C, Laachir et al. [70] found 200 °C (for the sample with the lowest onset temperature), Leitenburg et al. [71] found 327 °C, and Giordano et al. [72] found 227 °C. In spite of these uncertainties, we can state that doping with Ru lowers the onset temperature for the reduction by H_2. The presence of the Ru dopant makes the surface more reducible, hence a better oxidant.

The results of temperature-programmed reduction of $Ce_{0.95}Ru_{0.05}O_2$ with CO are shown in Fig. 11. CO oxidation starts at ~150 °C. At 250 °C, we begin to observe the production of H_2. The origin of this is not clear. There is water contamination in the system, but we see no change in the water signal when the H_2 signal appears. Therefore, we think that H_2 originates from the hydroxyls present on the surface and not from the reduction of water (by the reduced ceria surface [73]) or from the water–gas shift reaction ($CO + H_2O \rightarrow H_2 + CO_2$). From Fig. 9, we know that no H_2 is produced if we heat the surface in Ar, even though water and hydroxyls are present. Hence, H_2 production at 250 °C is connected to the fact that CO started reducing the surface at 150 °C; H_2 desorbs from the reduced surface. Apparently, the oxygen atoms

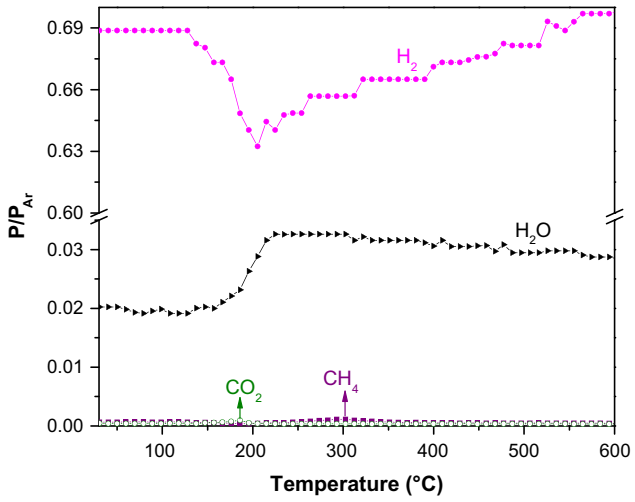

Fig. 10. Temperature-programmed reduction (TPR) of the $Ce_{0.95}Ru_{0.05}O_2$ catalyst made by combustion, exposed to H_2 (8 ml/min) and Ar (7 ml/min). Partial pressures are normalized by the partial pressure of Ar. The catalyst was pretreated in a flow of Ar at 500 °C for an hour.

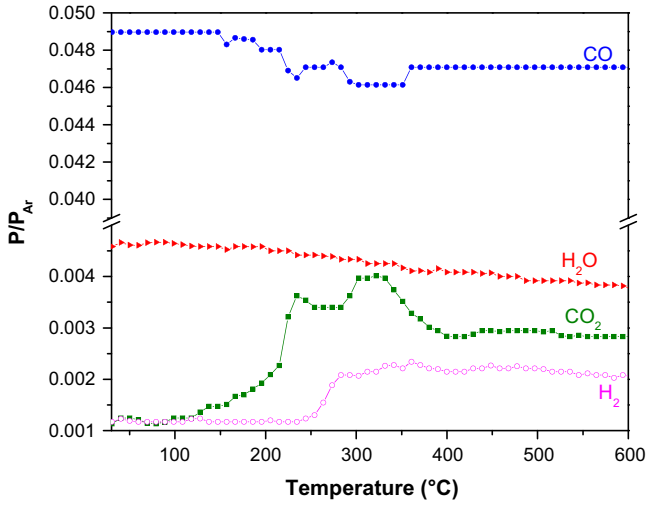

Fig. 11. Temperature-programmed reduction (TPR) of the $Ce_{0.95}Ru_{0.05}O_2$ catalyst made by combustion, exposed to CO (8 ml/min) and Ar (7 ml/min). The partial pressures are normalized by the partial pressure of Ar. The catalyst was pretreated in a flow of Ar at 500 °C for an hour.

on the reduced surface are more strongly bound to the surface and do not form water as easily as the fully oxidized surface; H_2 desorption is more facile than desorption as water. This assumption is supported by experiments performed by Bernal et al. [74] who have shown that H_2 adsorbed on reduced ceria desorbs as H_2 not as water. Moreover, Otsuka et al. [73] have shown that strongly reduced ceria converts water to hydrogen, a behavior that is very different from that of slightly reduced ceria for which the hydroxyls desorb as water not as H_2.

The reduction of pure ceria by CO has been studied by Aneggi et al. [75], who prepared six different ceria samples and found that reduction starts at ~227 °C for all of them. Other experiments [76] found that ceria having a large area per gram starts being reduced at room temperature, and the reduction becomes extensive at 200 °C; a sample with lower surface area per gram was reduced at higher temperature. Thus, pure ceria is reduced at lower temperature by CO than by H_2. However, one should keep in mind that ceria exposed to CO forms surface carbonates [77,78], and the surface being reduced by CO is not identical to the surface reduced by H_2. Of course the precise temperature where reduction begins depends on CO or H_2 pressure and on the preparation of the surface. If we compare the results shown in Fig. 11 with the literature results, it is not clear that doping with Ru makes ceria more reducible by CO. However, we are not aware of any TPR reduction of ceria with CO in which hydrogen is being produced. In this respect, Ru-doped ceria behaves differently than undoped ceria.

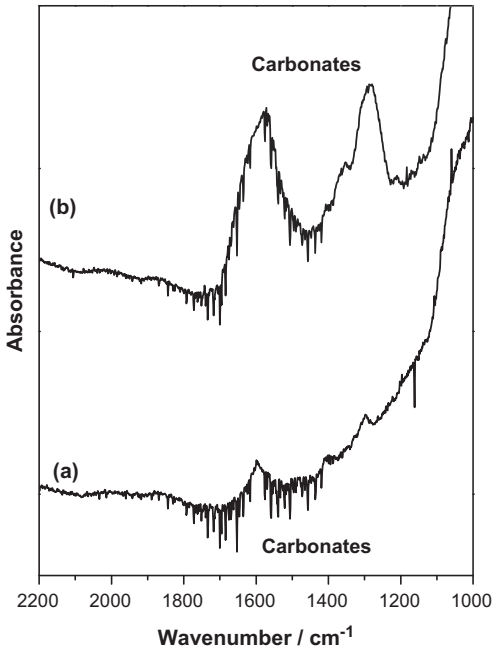

Fig. 12. DRIFT spectra of the $Ce_{0.95}Ru_{0.05}O_2$ catalyst made by combustion, under different treatment conditions. (a) DRIFT spectrum of the $Ce_{0.95}Ru_{0.05}O_2$ catalyst after it is heated to 500 °C, kept there for 20 min, and then cooled back to 35 °C in a flow of Ar (15 ml/min). (b) DRIFT spectrum of $Ce_{0.95}Ru_{0.05}O_2$ catalyst at 35 °C exposed to 5 ml/min of argon, 2 ml/min of CO_2, and 8 ml/min of H_2. Both spectra were taken after waiting for 10 min to reach the steady state.

7. IR spectroscopy

Diffuse Reflectance Infrared Fourier Transform Spectroscopy (DRIFT) was performed on $Ce_{0.95}Ru_{0.05}O_2$ under reaction conditions (Thermo Electron Corporation, Nicolet 4700). The catalyst was exposed to gases (5 ml/min for argon, 2 ml/min for CO_2 and 8 ml/min for H_2) by using an automated temperature controller (Harrick). Our intention was to identify reaction intermediates and determine their stability under reaction conditions.

The IR spectrum of the carbonates formed by exposing ceria to CO_2 has been published recently by Marbán et al. [79] in an article that also summarized the previous work [77–83]. They recommended the following assignments of the IR peak frequencies [79]: 1370, 1351–1367, 1464, 1517 cm^{-1} for the monodentate carbonate; 850, 854, 1305, 1297, 1588, 1586 cm^{-1} for the bidentate carbonate; and 1305, 1316, 1510 cm^{-1} for bicarbonate.

Fig. 12 shows the DRIFT spectrum of the as-prepared $Ce_{0.95}Ru_{0.05}O_2$ catalyst. The catalyst was kept for 1 h at 500 °C in a flow

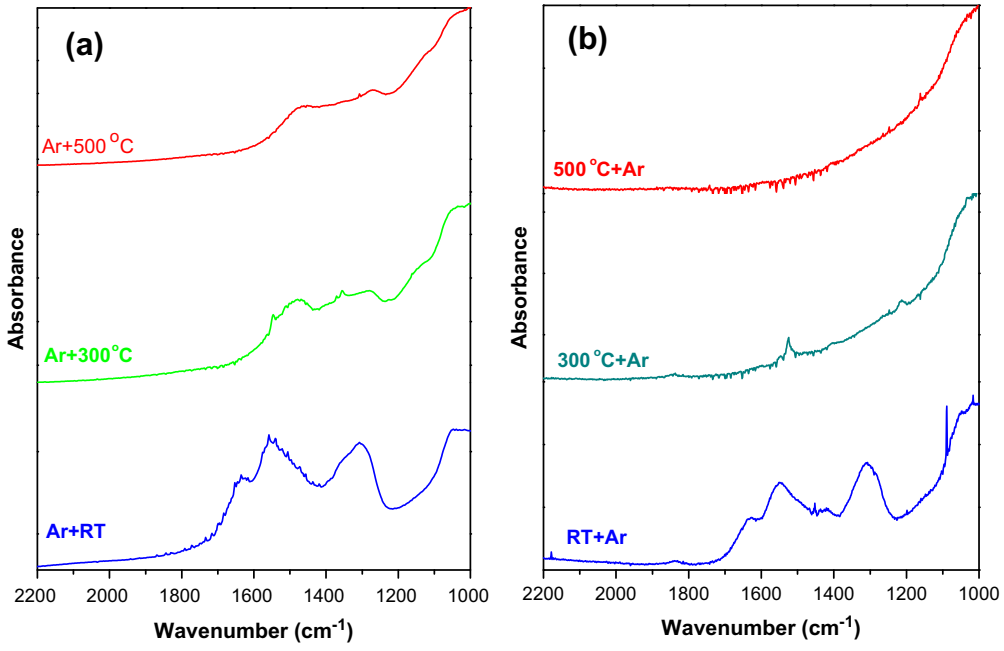

Fig. 13. DRIFT spectra of CeO_2 and $Ce_{0.95}Ru_{0.05}O_2$ catalyst made by combustion, under different temperature conditions. (a) DRIFT spectra of CeO_2 at room temperature, 300 °C, and 500 °C; (b) DRIFT spectra of $Ce_{0.95}Ru_{0.05}O_2$ at room temperature, 300 °C and 500 °C in the flow of Ar (15 ml/min). It takes 10 min to reach the steady state.

of high-purity Ar, to remove gases other than Ar from the reactor. Then, it was cooled to 35 °C in about 30 min. The IR spectrum, taken after cooling, is shown in Fig. 12a. It has three small peaks. The one at ~1600 cm^{-1} has a higher frequency than any of the assignments listed above for carbonates [79]. The one at ~1400 cm^{-1} might be monodentate carbonate, and the one at ~1250 cm^{-1} is closest to a frequency assigned to the bidentate carbonate.

The reason for the presence of the carbonates on the surface can be determined by examining Fig. 13b, which shows that there is no carbonate band when $Ce_{0.95}Ru_{0.05}O_2$ is exposed to Ar at 500 °C (the spectrum was taken after the mass spectrometer detects no CO_2 in the gases coming out of the reactor). This means that the carbonates on the $Ce_{0.95}Ru_{0.05}O_2$ surface are not stable at 500 °C when the surface is exposed to Ar. Therefore, the carbonates seen in Fig. 12a must have been formed when we cooled the surface, in "pure" Ar, from 500 °C to 35 °C (the temperature at which the spectrum in Fig. 12a was taken). Since cooling was done in a flow of high-purity Ar, these results show that the trace CO_2 impurity in Ar is sufficient to form carbonates on the $Ce_{0.95}Ru_{0.05}O_2$ surface.

Fig. 12b shows the spectrum obtained after the catalyst used in the measurements reported in Fig. 12a was exposed, for 10 min, at 35 °C, to a steady flow of a gas containing CO_2 (2 ml/min), H_2 (8 ml/min), and Ar (5 ml/min). The concentration of the carbonates is increased substantially by exposure to CO_2 and H_2. The carbonate peaks merge, probably due to inhomogeneous broadening, to form two bands. A deconvolution of these bands is not reliable, and we do not attempt to quantify how much bicarbonate, or monodentate carbonate, or bidentate carbonate is present on the surface. In what follows, we call these two broad peaks the 'carbonate bands'.

Prior work on CO_2 hydrogenation [1–5] by supported metal catalysts suggested that in many cases, CO_2 is first reduced to CO which is then converted to alkanes by a Fischer–Tropsch reaction. Often a formate intermediate is invoked to explain the hydrogenation of CO. We do not see any IR adsorption in the region between 2700 and 3100 cm^{-1} where formate bands are expected [79].

To examine the extent to which the chemistry of the $Ce_{0.95}Ru_{0.05}O_2$ surface differs from that of CeO_2, we used IR spectroscopy to monitor carbonate decomposition with temperature. Fig. 13 shows the carbonate bands in the IR spectra of CeO_2 (Fig. 13a) and of $Ce_{0.95}Ru_{0.05}O_2$ (Fig. 13b), taken while the surface was maintained at constant temperature, in a flow of argon. In the IR experiments, the steady state is reached in 10 min after reaching at the required temperature. At room temperature, the carbonate bands are intense for both materials. When the temperature is 300 °C, the intensity of the carbonate band on CeO_2 decreases and it disappears for $Ce_{0.95}Ru_{0.05}O_2$. If the Ru dopant affects only a few oxygen atoms next to it and if there are only a few Ru atoms on the surface, then the surface would have oxygen atoms that behave like those of pure ceria. The carbonates formed on these atoms would not decompose at 300 °C. The fact that the carbonate signal disappears at 300 °C on $Ce_{0.95}Ru_{0.05}O_2$ suggests either that there is enough Ru on the surface to affect the majority of the oxygen atoms or that Ru in the bulk affects the chemistry of the surface, or both.

During this experiment, the solids are exposed to argon, which contains enough CO_2 to contaminate the sample. Because the carbonate bands disappear at 300 °C, from the $Ce_{0.95}Ru_{0.05}O_2$, we conclude that, on this material, the rate of carbonate decomposition exceeds the rate of contamination with CO_2. This is not the case for pure ceria. Therefore, the decomposition rate of the carbonates on $Ce_{0.95}Ru_{0.05}O_2$ is higher than that of the carbonates on CeO_2. There are still carbonates on ceria at 500 °C (which is consistent with previous work [77]), and none is seen on $Ce_{0.95}Ru_{0.05}O_2$. Doping the oxide with Ru significantly affects the stability of the carbonates.

In Fig. 14, we show the *in situ* IR spectra when the system is exposed to CO_2 (2 ml/min), H_2 (8 ml/min), and Ar (5 ml/min) and is held at constant temperature. The spectra were taken after the system reached steady state. A spectrum taken over a wider range of wavelengths than that shown in Fig. 14 shows strong absorbance from gas-phase CO_2 and CH_4; we only show the spectral region containing signals from the surface species. The sharp peak marked with a star is due to gas-phase methane.

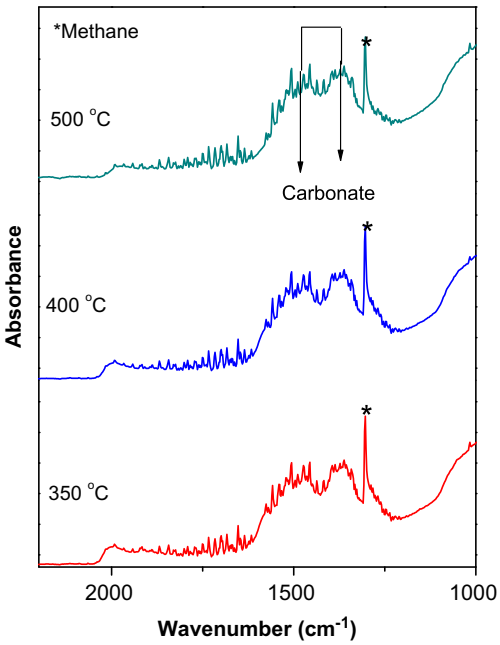

Fig. 14. DRIFT spectra of the $Ce_{0.95}Ru_{0.05}O_2$ catalyst made by combustion, at different temperatures. The catalyst was exposed to Ar (5 ml/min), CO_2 (2 ml/min), and H_2 (8 ml/min) at 350, 400, and 500 °C. It takes 10 min to reach the steady state at each temperature.

In all spectra shown in Fig. 14, we see a weak band at ~2000 cm^{-1}. We are unable to identify the species responsible for this band. The spectrum of CO adsorbed on ceria has peaks [77] at 2177 and 2156 cm^{-1}. The peaks for the carbonates formed by CO adsorption have frequencies [77] below 1562 cm^{-1}. It appears that the feature at ~2000 cm^{-1} has not been seen previously on ceria, and it is unique to $Ce_{0.95}Ru_{0.05}O_2$.

We have performed DFT calculations for CO adsorbed on the surface of $Ce_{1-x}Ru_xO_2$(1 1 1) in which the Ru atom replaces a Ce atom in the surface layer and an oxygen vacancy is present near the Ru dopant. We looked at a system having an oxygen vacancy because H_2 reduces $Ce_{1-x}Ru_xO_2$ at the temperatures at which the methanation reaction takes place (see Fig. 10). In the calculations, the vacancy was formed by removing the oxygen atom that has the lowest binding energy to the surface. We found two low-energy states for CO binding to $Ce_{1-x}Ru_xO_2$ that has an oxygen vacancy. The structure of the state having the lowest energy is shown in Fig. 15. In the upper part, the unit cell of the slab used in the calculation is shown, as seen from above (Fig. 15a) and from the side (Fig. 15b); each lower part shows a schematic of the bonding as well as the positions of a small number of atoms in the neighborhood of the C atom (at the positions they have in the slab calculation). The carbon atom of the adsorbed CO molecule (in gray) binds to the Ru dopant (blue[1]) and to an oxygen atom from the second surface layer (orange). Some information about bonding in this system is given in Table 2. It is reasonable to think that the adsorbed CO forms a "CO_2 molecule" since the two C–O bonds are of equal length (Table 2). The formation of this complex lowers the energy by 3.41 eV (with respect to CO in the gas phase and $Ce_{1-x}Ru_xO_2$ having

[1] (For interpretation of color in Fig. 15, the reader is referred to the web version of this article.)

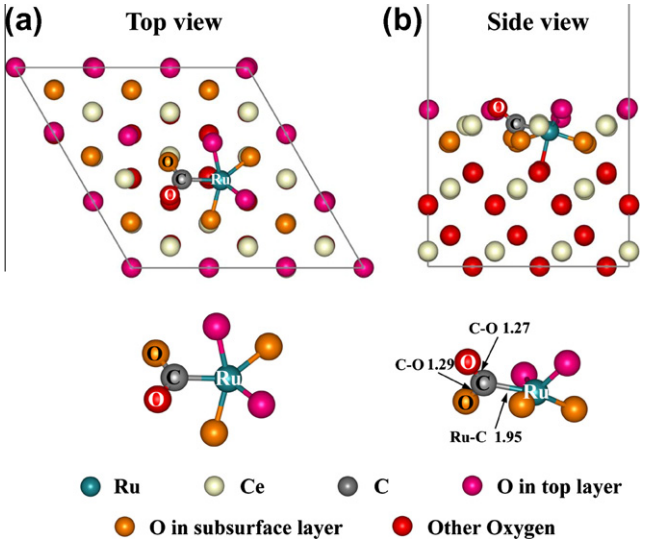

Fig. 15. One of the states reached when CO adsorbs on reduced $Ce_{1-x}Ru_xO_2$ to form a "CO_2 molecule" with the carbon atom bonded to the Ru dopant. (a) Top view of the supercell used in the calculation. For clarity, we show a cluster cut from the supercell without changing the positions of the atoms. (b) The side view of the supercell used in the calculation. Below we show, for clarity, a cluster cut from the supercell without changing the positions of the atoms. The oxygen atom from CO is in red with white label. (For interpretation of the references to colour in this figure legend, the reader is referred to the web version of this article.)

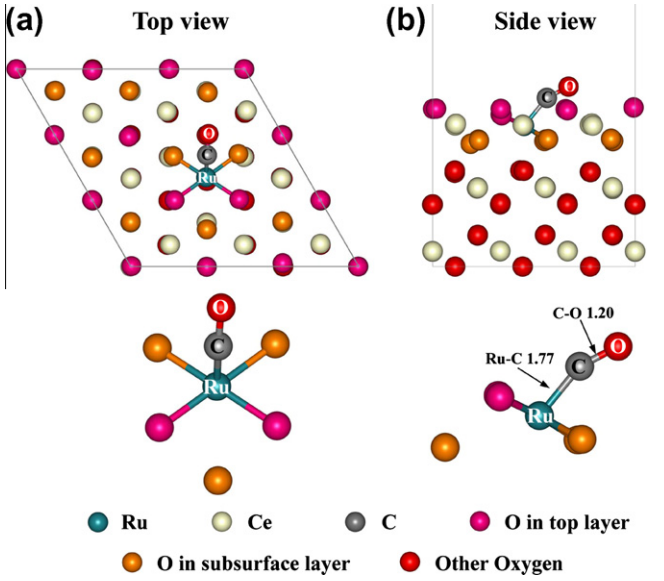

Fig. 16. Another state reached when CO adsorbs on reduced $Ce_{1-x}Ru_xO_2$ to form a "carbonyl" by binding to the Ru dopant. (a) The top view of the supercell used in the calculation. Below it we show, for clarity, a cluster cut from the supercell, without changing the positions of the atoms. (b) The side view of the supercell with a cluster cut from it below it. The oxygen atom from CO is labeled by O.

Table 2
Ru–CO is the compound in Fig. 15 where CO is bonded to Ru. Ru–CO_2 is the compound in Fig. 14 where CO makes a bond with Ru and with an O atom to form a "CO_2 molecule". For Ru–CO: E_b is the binding energy of gas-phase CO to the reduced, Ru-doped ceria, to form Ru–CO; ω_1 is the C–O frequency; ω_2 is the C–Ru frequency; d_1 is the C–O bond length; and d_2 is the Ru–C bond length. For Ru–CO_2: E_b is the binding energy of CO to the reduced, Ru-doped ceria to form Ru–CO_2; ω_1 and ω_2 are frequencies of the symmetric and antisymmetric vibrations of the CO_2 group; d_1 and d_2 are the lengths of the two C–O bonds in the CO_2 group; and d_3 is the Ru–C length.

Compound	E_b (eV)	ω_1 (cm^{-1})	ω_2 (cm^{-1})	d_1 (Å)	d_2 (Å)	d_3 (Å)
Ru–CO	−2.32	1825	606	1.20	1.77	–
Ru–CO_2	−3.41	1476	1276	1.27	1.29	1.96

an oxygen vacancy). The two frequencies associated with the O–C–O group are approximately 1476 cm^{-1} and 1276 cm^{-1} and are caused by a symmetric and antisymmetric stretch of the O–C–O group.

The second possibility for CO binding is shown in Fig. 16. The carbon atom of CO binds to the Ru dopant to form a sort of "carbonyl". The binding energy is 2.32 eV, the CO stretching frequency is 1825 cm^{-1}, and the stretching frequency of the C–Ru bond is 606 cm^{-1} (Table 2). Within the accuracy of DFT, the CO molecule binds very weakly to the oxygen atoms on the surface and such a species would not be present at the high temperatures at which the 2000 cm^{-1} band is present in Fig. 14.

We have also calculated the vibrational frequency of a CO_2 molecule adsorbed at the site of an oxygen vacancy (near the Ru dopant) and found that its highest vibrational frequency is 1847 cm^{-1}.

These calculations suggest that the band at ~2000 cm^{-1} in Fig. 14 does not originate from CO or CO_2 adsorbed on the reduced $Ce_{1-x}Ru_xO_2$. In a further attempt to determine the origin of this band, we took the IR spectrum of the reduced $Ce_{0.95}Ru_{0.05}O_2$ surface exposed to CO. We see the carbonate bands and also very small peaks whose frequencies are close to the ones predicted by the calculations. However, the peaks are too small to give convincing proof that the compounds calculated have been observed experimentally. More important is the fact that when CO is adsorbed on reduced $Ce_{1-x}Ru_xO_2$, the IR spectrum has no band at 2000 cm^{-1}.

We conclude that the nature of the band at ~2000 cm^{-1} is uncertain. In the next section, we show that in spite of the presence of this band, it very unlikely that some form of CO is an intermediate in the methanation reaction.

8. CO methanation by H_2

Prior publications on CO_2 hydrogenation suggested that CO_2 is reduced to CO, which is then hydrogenated through a Fischer–Tropsch process. To determine whether this mechanism is consistent with our observations on $Ce_{0.95}Ru_{0.05}O_2$, we performed temperature-programmed reaction of CO with H_2, on $Ce_{0.95}Ru_{0.05}O_2$. We reasoned that if CO is an intermediate in CO_2 methanation by $Ce_{0.95}Ru_{0.05}O_2$, then this catalyst should methanate CO. We find, essentially, no activity for CO methanation (Fig. 17). A very small amount of methane is produced at 350 °C, but even at 600 °C methane production is very small. Compare this to the methanation of CO_2 (Figs. 5 and 7) for which the $Ce_{0.95}Ru_{0.05}O_2$ begins producing methane at 300 °C with a much larger yield than that obtained by CO hydrogenation at 600 °C. We conclude that CO_2 methanation does not take place through a CO intermediate.

It is interesting to note that when we expose $Ce_{0.95}Ru_{0.05}O_2$ to CO and H_2, the oxidation of CO to CO_2 starts at 75 °C. This is lower than the temperatures at which CO alone is oxidized (~175 °C, Fig. 11), and lower than the temperature at which H_2 alone is oxidized (~135 °C, Fig. 10). It appears that the mixture of CO + H_2 is a better reductant than either CO or H_2.

In Fig. 18, we show the gas-phase methane and surface hydroxyls for $Ce_{0.95}Ru_{0.05}O_2$ exposed to a flow of CO (3 ml/min), H_2 (9 ml/min), and Ar (3 ml/min), at 300, 400 and 500 °C. We compare the observed DRIFT spectra to the spectrum of the same catalyst exposed to a flow CO_2 (2 ml/min), H_2 (8 ml/min), and Ar (5 ml/min), at 300 °C. All spectra were taken after the system reached steady state. Practically no methane is observed for CO + H_2 at 300 and 400 °C and very little is seen at 500 °C. The hydroxyl signal is very weak compared to that obtained for CO_2 + H_2. The IR spectra show that $Ce_{0.95}Ru_{0.05}O_2$ does not catalyze CO hydrogenation under conditions for which it is active for CO_2 hydrogenation.

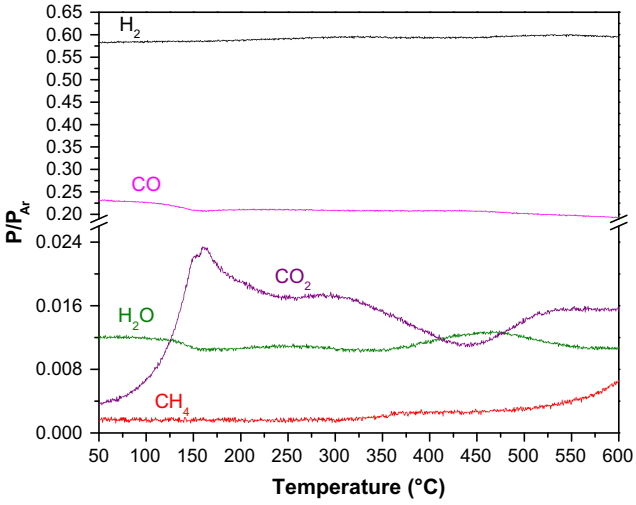

Fig. 17. Temperature-programmed reaction for the reaction of CO with H_2, catalyzed by the $Ce_{0.95}Ru_{0.05}O_2$ catalyst made by combustion. The $Ce_{0.95}Ru_{0.05}O_2$ catalyst was exposed to CO (3 ml/min), H_2 (9 ml/min), and Ar (3 ml/min). The partial pressures are normalized by the partial pressure of Ar. The data indicate that CO + H_2 is a better reductant than either CO or H_2 individually. CO_2 formation starts at 50 °C. No methane formation is observed up to 550 °C.

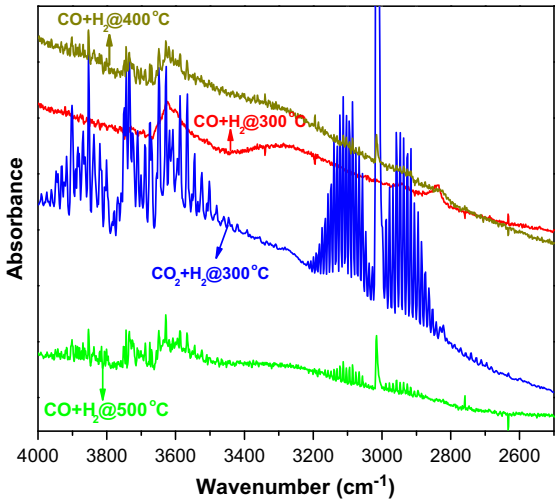

Fig. 18. DRIFT spectra of the $Ce_{0.95}Ru_{0.05}O_2$ catalyst made by combustion, under different reaction conditions. DRIFT spectra of $Ce_{0.95}Ru_{0.05}O_2$ catalyst exposed to CO (3 ml/min), H_2 (9 ml/min), and Ar (3 ml/min) at three temperatures: 300, 400, and 500 °C. Comparison is made with the $Ce_{0.95}Ru_{0.05}O_2$ catalyst exposed to Ar (5 ml/min), CO_2 (2 ml/min), and H_2 (8 ml/min) at 300 °C.

It is interesting to note that the hydroxyl signal is very weak when the surface is exposed to CO + H_2, and it is substantial when it is exposed to CO_2 + H_2. The surface exposed to CO and H_2 is reduced more than the one exposed to CO_2 and H_2. The weak hydroxyl signal for CO + H_2 suggests that on the reduced surface, the hydrogen does not make hydroxyls. One might think of the reduced surface as consisting on patches of oxygen and patches of ionic cerium. When such patches are present, it may be that the oxygen is less active in forming hydroxyls and the hydrogen may dissociate on cerium patches and make Ce–H bonds. This may explain why fewer hydroxyls are observed on the surface and is consistent with the observation that when reduced ceria is exposed to hydrogen and then heated H_2 is desorbed, not water [74]. A simpler explanation for the reduced number of hydroxyls may be that the reduced surface has fewer oxygen atoms for the H to bind to.

9. The local and the global effect of a dopant

So far our previous computational work has considered the effect a dopant has on the oxygen atoms nearby [84–90] or on the molecules adsorbed on it [91]. In these cases, the dopant has a "chemical effect" since its role is to modify locally the strength of chemical bonds.

In the case of $Ce_{0.95}Ru_{0.05}O_2$, a good fraction of Ru atoms are located in the bulk, and calculations indicate that the Ru atoms in the surface region (i.e. accessible to XPS) prefer to be located in the second Ce layer. Therefore, it is likely that many oxygen sites on the surface might be far from a Ru atom. If they are unaffected by dopants, they should behave like the oxygen atoms on an undoped ceria surface. In particular, carbonates should be present on the surface up to 500 °C. We do not observe carbonates on $Ce_{0.95}Ru_{0.05}O_2$ even at 300 °C, a temperature at which they are abundant on the undoped ceria surface. This suggests that the Ru dopants might also have a long-range effect. Since it is impossible to estimate the Ru concentration in the surface layer, we cannot assert that such an effect is proven by our experiments. Nevertheless, we discuss here the possibility that a dopant has a "global effect" and modifies the reactivity at distant surface sites.

In a simplified model, this effect occurs because the dopant changes the Fermi level of the oxide and this can affect the charge rearrangement taking place during a reaction. To understand qualitatively how this works, consider the conversion of an adsorbed intermediate A to an adsorbed intermediate B. The simplest example would be the desorption of a CO molecule bound to the surface (system A) to create a CO_2 molecule in the gas and an oxygen vacancy on the surface (system B). In many cases when such a reaction takes place, the energies of the orbitals in the band gap change: the filled and empty orbitals of A (in the gap) have different energies than the localized orbitals of B (in the gap). In particular, this is the case when CO reacts with the solid surface to form CO_2 since an oxygen vacancy is left behind, which is known to produce new states in the gap [44,46,92]. It is likely to be the case in general, because adsorbates tend to have some localized frontier orbitals whose energy is located in the gap.

Let us assume, for simplicity, that when A is present on the surface, there is no orbital in the band gap. This is, for example, the case when the reaction A → B is the formation of an oxygen vacancy on the surface [44]. Let us denote by ε_e the energy of an empty orbital created when B is formed, and denote by ε_F the Fermi energy. If $\varepsilon_F > \varepsilon_e$, an electron will be transferred to B when the reaction A → B takes place. This will happen regardless of whether the oxide is doped or not. One could think, qualitatively, of the formation of B as consisting of two successive steps: (a) in the first step, the chemical bonds at the surface are rearranged (or broken) so that A is converted to B, and this requires the "chemical" energy ΔE; (b) in addition, an electron is transferred from ε_F to ε_e with the energy gain $\varepsilon_F - \varepsilon_e$. As long as $\varepsilon_F > \varepsilon_e$ the energy to go from A to B is $\Delta E - |(\varepsilon_F - \varepsilon_e)|$; the energy $|(\varepsilon_F - \varepsilon_e)|$ gained through electron transfer lowers the total reaction energy. This equation shows that a dopant that changes the Fermi energy ε_F affects the reaction energy. Lowering the reaction energy often results in lowering the activation energy (Evans–Polanyi rule), so both the thermodynamic and the kinetic properties of the surface are affected.

Since the Fermi energy is a global property (i.e. the Fermi energy is the same at any surface site – we exclude the presence of inhomogeneous electric fields in which case we would need to use the electrochemical potential as a global quantity [[93], Chapter 29]), the presence of the term $\varepsilon_F - \varepsilon_e$ in the reaction energy affects it globally (regardless of the distance between the dopant and the reaction site).

Similarly, if the reaction A → B creates a localized, filled state in the gap, having an energy ε_f, and if $\varepsilon_f > \varepsilon_F$, the reaction will cause an electron transfer from the filled orbital of B to the Fermi level; the energy of the reaction is lowered by the amount $\varepsilon_f - \varepsilon_F$. Again, by changing the position of the Fermi level, the dopant can affect the reaction energy. The important point is that through this mechanism, a dopant can affect the energy of a reaction taking place anywhere on the surface, regardless of the dopant's location. We call this a 'global effect' to contrast it with the change caused in the reactivity of the sites *adjacent* to the dopant, a change present because the dopant modifies the strength of the chemical bonds around it.

This kind of global effect has been discussed in the semiconductor literature in connection with the formation of bulk defects and, in particular, with the formation of oxygen vacancies [94–96]. If the Fermi energy of the semiconductor is sufficiently high, negatively charged oxygen vacancies are stable; if the Fermi energy is very low, positively charged vacancies are formed; neutral vacancies are formed when the Fermi energy is in between. The present discussion extends these concepts to chemical reactions on a surface, among which oxygen-vacancy formation is a particular case. While the model has a number of simplifications, it clearly provides a mechanism through which dopants can have a long-range effect.

This discussion has focused on reaction energies, and it is therefore relevant to a thermodynamic analysis which is trying to establish the effect of remote dopants on the equilibrium concentration of A and B. The kinetic aspects of the charge transfer process are also interesting. If a dopant is far from the site on which A → B takes place (e.g. the dopant is in the bulk and the reaction takes place on the surface), the charge transfer cannot take place by electron tunneling from the donor to the acceptor and several steps need to be invoked. An electron from the donor (which could be either the dopant or B) is thermally excited to the conduction band where it will form a polaron, which hops from site to site until its electron wave function overlaps with the empty orbital of the acceptor and the localization of the electron on the acceptor can take place. The kinetics involves electron excitation, polaron formation, the electron–hole separation, the polaron migration, and the transfer of the electron to the acceptor. Obviously, the global effect is most pronounced for "shallow donors" [97] for which the HOMO is closest to the conduction band and which are easily ionized thermally.

These arguments indicate that in dealing with the equilibrium and the kinetics of A → B, we should take into account the electron transfer aspects discussed earlier. This means that the partition functions used in either equilibrium calculations or the transition state theory should include the electronic degrees of freedom. We must consider the population of the neutral donors and that of the charged donors as well as the population of the neutral and charged acceptors.

10. Summary

We have found that the activity and the selectivity of the $Ce_{0.95}Ru_{0.05}O_2$ catalyst for CO_2 methanation is comparable to that of the best catalysts reported previously. A quantitative comparison is difficult because in most of the available experiments (including ours), the quantitative description of the activity of the catalyst depends on the reactor used in the measurements.

Ceria doped with Ni or Co is not selective: it catalyzes methanation and the reverse water–gas shift reaction. Pd-doped ceria produces only CO.

It is always difficult to prove that the catalyst is a doped oxide. Our electron microscopy and XRD measurements suggest that Ru is incorporated into the ceria lattice. The XPS measurements indicate that Ru is ionic and is present in the surface region. The DFT calculations show that $Ce_{1-x}Ru_xO_2$ has the lowest energy when the Ru atoms are in the second Ce layer (of the CeO_2(1 1 1) surface). Therefore, if the Ru atoms are close to being in chemical equilibrium, most of them are likely to be in the surface region. Given the surface area and the number of surface sites and given the number of Ru atoms we add to the system, we conclude that many Ru atoms are in the bulk. This is supported by the XRD measurements which show that $Ce_{0.95}Ru_{0.05}O_2$ has the ceria structure with a modified lattice constant, which can only happen if a substantial fraction of the Ru atoms are in the bulk.

The most convincing proof that a doped oxide has been prepared is to show that the chemistry of the surface is different from that of other structures that might have been synthesized. To this end, we prepared a catalyst consisting of metallic Ru clusters supported on ceria, which has the same amount of Ru as the one prepared by combustion (which we assume to yield doped ceria). The two catalysts have very different activity and selectivity for CO_2 methanation. A variety of temperature-programmed reaction measurements show that the catalyst made by the combustion method is more reducible than ceria.

In much of the literature on CO_2 methanation, it is assumed (and sometimes proven) that the hydrogenation of CO_2 consists of the reduction of CO_2 to CO, followed by the conversion to alkanes by a Fischer–Tropsch process. This assumption guided previous research: most catalysts tried for CO_2 methanation were those active for the Fischer–Tropsch reaction. Our TPR measurements show that CO + H_2 react to produce CO_2 and water and practically no methane; therefore, gas-phase CO is not a reaction intermediate for the methanation of CO_2 by $Ce_{0.95}Ru_{0.05}O_2$.

In the past, we have used density functional calculations to try to classify the possible roles played by substitutional doping of oxides. We have found the following qualitative rules: (1) Dopants that have a lower valence than the cation replaced in the host oxide (Li-doped MgO, La-doped ceria, etc.) tend to weaken the bonds of the oxygen atoms to the surface. This makes the oxygen atoms more reactive and they engage more readily in catalysis by a Mars–van Krevelen mechanism [84,85,87–89,91]. We have pointed out however a "moderation principle": if the dopant makes the oxygen atoms in the surface layer too reactive, the system is a good oxidant but not a good oxidation catalyst; the oxygen atoms are easily consumed by the reductant, with the formation of oxygen vacancies, but these vacancies are not filled rapidly by gas-phase oxygen. (2) Dopants that have a higher valence than the cation they replace tend to bind the oxygen atoms in their neighborhood more tightly. Therefore, they do not enhance oxidation by the Mars–van Krevelen mechanism. However, in most cases, these dopants adsorb O_2 from the gas phase and activate it. In these systems, the oxidation is due to the adsorbed O_2 (an "anti-Mars–van Krevelen" mechanism) [91]. (3) The present work adds to these a third mechanism. Hydrogen reduces the surface at a temperature well below the temperature at which methanation occurs. Therefore, the methanation reaction takes place on the reduced surface and the role of the dopant is to facilitate the reduction of the oxide. The addition of oxygen in the feed "poisons" the reaction by annihilating the oxygen vacancies.

There are by now many examples in which a very low dopant concentration modifies substantially the reactivity of an oxide (and by extension of a sulfide or a halide) catalyst, especially when the dopant has a tendency to segregate at the surface either because it has lower energy there or because its energy in the surface layer is lowered by interaction with the adsorbed molecules. Using precursors having 99.99% purity introduces unknown dopants in the system. These can diminish or enhance the effect of the dopants added intentionally and make it difficult to perform control

experiments with genuinely pure oxides, which are needed for understanding how a dopant affects the catalytic properties of an oxide.

Acknowledgments

This research was supported in part by the US Department of Energy under Grant No. DE-FG02-89ER140048 and the University of California Lab Fee Research Program under Grant No. UCOP09-LR-08-116809. We made use of the computer facility of the California NanoSystems Institute funded in part by the National Science Foundation. Use of the Center for Nanoscale Materials was supported by the US Department of Energy, Office of Science, Office of Basic Energy Sciences, under Contract No. DE-AC02-06CH11357. We are grateful for useful conversations with Alan Derk, who suggested that the reduced doped oxide is the catalyst, and with Matthias Scheffler, with whom we discussed the distinction between the global and the chemical effects of a dopant.

References

[1] S.B. Wang, Z.H. Zhu, Energy Fuels 18 (2004) 1126.
[2] T. Sakakura, J.C. Choi, H. Yasuda, Chem. Rev. 107 (2007) 2365.
[3] P. Sai Prasad, J. Bae, K.-W. Jun, K.-W. Lee, Catal. Surv. Asia 12 (2008) 170.
[4] M. Aresta, A. Dibenedetto, Dalton Trans. (2007) 2975.
[5] I. Omae, Catal. Today 115 (2006) 33.
[6] F. Solymosi, A. Erdöhelyi, J. Mol. Catal. 8 (1980) 471.
[7] C. Schild, A. Wokaun, R.A. Koeppel, A. Baiker, J. Phys. Chem. 95 (1991) 6341.
[8] S.-S. Nam, S.-J. Lee, H. Kim, K.-W. Jun, M.-J. Choi, K.-W. Lee, Energy Convers. Manage. 38 (1997) 397.
[9] H. Ando, Q. Xu, M. Fujiwara, Y. Matsumura, M. Tanaka, Y. Souma, Catal. Today 45 (1998) 229.
[10] M. Lee, J. Lee, C. Chang, Bull. Chem. Soc. Jpn. 62 (1989) 2756.
[11] M.-J. Choi, J.-S. Kim, H.-K. Kim, S.-B. Lee, Y. Kang, K.-W. Lee, Korean J. Chem. Eng. 18 (2001) 646.
[12] J. Barrault, C. Forquy, J.C. Menezo, R. Maurel, React. Kinet. Catal. Lett. 17 (1981) 373.
[13] Y.M. Yu, J.H. Fei, Y.P. Zhang, X.M. Zheng, Chin. Chem. Lett. 17 (2006) 1097.
[14] T. Riedel, M. Claeys, H. Schulz, G. Schaub, S.-S. Nam, K.-W. Jun, M.-J. Choi, G. Kishan, K.-W. Lee, Appl. Catal. A: Gen. 186 (1999) 201.
[15] Y. Zhang, G. Jacobs, D.E. Sparks, M.E. Dry, B.H. Davis, Catal. Today 71 (2002) 411.
[16] T. Riedel, H. Schulz, G. Schaub, K.-W. Jun, J.-S. Hwang, K.-W. Lee, Top. Catal. 26 (2003) 41.
[17] J.S. Kim, S.B. Lee, M.C. Kang, K.W. Lee, M.J. Choi, Y. Kang, Korean J. Chem. Eng. 20 (2003) 967.
[18] S.-R. Yan, K.-W. Jun, J.-S. Hong, M.-J. Choi, K.-W. Lee, Appl. Catal. A: Gen. 194–195 (2000) 63.
[19] J.S. Hwang, K.-W. Jun, K.-W. Lee, Appl. Catal. A: Gen. 208 (2001) 217.
[20] J.S. Hong, J.S. Hwang, K.W. Jun, J.C. Sur, K.W. Lee, Appl. Catal. A: Gen. 218 (2001) 53.
[21] P.H. Choi, K.-W. Jun, S.-J. Lee, M.-J. Choi, K.-W. Lee, Catal. Lett. 40 (1996) 115.
[22] M. Fujiwara, R. Kieffer, H. Ando, Y. Souma, Appl. Catal. A: Gen. 121 (1995) 113.
[23] M. Fujiwara, R. Kieffer, H. Ando, Q. Xu, Y. Souma, Appl. Catal. A: Gen. 154 (1997) 87.
[24] J.-S. Kim, S. Lee, S.-B. Lee, M.-J. Choi, K.-W. Lee, Catal. Today 115 (2006) 228.
[25] N.M. Gupta, V.S. Kamble, K.A. Rao, R.M. Iyer, J. Catal. 60 (1979) 57.
[26] K.R. Thampi, J. Kiwi, M. Graetzel, Nature 327 (1987) 506.
[27] T. Abe, M. Tanizawa, K. Watanabe, A. Taguchi, Energy Environ. Sci. 2 (2009) 315.
[28] J.-N. Park, E.W. McFarland, J. Catal. 266 (2009) 92.
[29] J.G. Highfield, M. Prairie, A. Renken, Catal. Today 9 (1991) 39.
[30] M.R. Prairie, A. Renken, J.G. Highfield, K.R. Thampi, M. Grätzel, J. Catal. 129 (1991) 130.
[31] M.R. Prairie, J.G. Highfield, A. Renken, Chem. Eng. Sci. 46 (1991) 113.
[32] G.M. Shashidhara, M. Ravindram, React. Kinet. Catal. Lett. 46 (1992) 365.
[33] N.M. Gupta, V.S. Kamble, R.M. Iyer, K.R. Thampi, M. Grätzel, Catal. Lett. 21 (1993) 245.
[34] N.M. Gupta, V.S. Kamble, V.B. Kartha, R.M. Iyer, K.R. Thampi, M. Grätzel, J. Catal. 146 (1994) 173.
[35] D. Li, N. Ichikuni, S. Shimazu, T. Uematsu, Appl. Catal. A: Gen. 172 (1998) 351.
[36] D. Li, N. Ichikuni, S. Shimazu, T. Uematsu, Appl. Catal. A: Gen. 180 (1999) 227.
[37] M. Marwood, R. Doepper, M. Prairie, A. Renken, Chem. Eng. Sci. 49 (1994) 4801.
[38] M. Marwood, F. Van Vyve, R. Doepper, A. Renken, Catal. Today 20 (1994) 437.
[39] J.M. Rynkowski, T. Paryjczak, A. Lewicki, M.I. Szynkowska, T.P. Maniecki, W.K. Jóźwiak, React. Kinet. Catal. Lett. 71 (2000) 55.
[40] S. Scirè, C. Crisafulli, R. Maggiore, S. Minicò, S. Galvagno, Catal. Lett. 51 (1998) 41.
[41] P. Sabatier, J.B. Senderens, C. R. Acad. Sci. 134 (1902) 689.
[42] M.S. Hegde, G. Madras, K.C. Patil, Acc. Chem. Res. 42 (2009) 704.
[43] M.W. McQuire, C.H. Rochester, J. Chem. Soc. Faraday Trans. 89 (1993) 1117.
[44] M.V. Ganduglia-Pirovano, A. Hofmann, J. Sauer, Surf. Sci. Rep. 62 (2007) 219.
[45] G. Pacchioni, J. Chem. Phys. 128 (2008) 182505.
[46] H.Y. Li, H.F. Wang, X.Q. Gong, Y.L. Guo, Y. Guo, G.Z. Lu, P. Hu, Phys. Rev. B 79 (2009) 193401.
[47] C. Loschen, J. Carrasco, K.M. Neyman, F. Illas, Phys. Rev. B 75 (2007) 035115.
[48] S.L. Dudarev, G.A. Botton, S.Y. Savrasov, C.J. Humphreys, A.P. Sutton, Phys. Rev. B 57 (1998) 1505.
[49] D.A. Andersson, S.I. Simak, B. Johansson, I.A. Abrikosov, N.V. Skorodumova, Phys. Rev. B 75 (2007) 035109.
[50] G. Kresse, J. Furthmüller, Comput. Mater. Sci. 6 (1996) 15.
[51] G. Kresse, J. Furthmüller, Phys. Rev. B 54 (1996) 11169.
[52] G. Kresse, J. Hafner, Phys. Rev. B 48 (1993) 13115.
[53] G. Kresse, J. Hafner, Phys. Rev. B 49 (1994) 14251.
[54] P. Singh, M.S. Hegde, Chem. Mater. 21 (2009) 3337.
[55] S.-B. Han, Y.-J. Song, J.-M. Lee, J.Y. Kim, W. Park, Electrochem. Commun. 10 (2008) 1044.
[56] D.R. Rolison, P.L. Hagans, K.E. Swider, J.W. Long, Langmuir 15 (1999) 774.
[57] P.C.H. Mitchell, C.E. Scott, J.-P. Bonnelle, J.G. Grimblot, J. Catal. 107 (1987) 482.
[58] E.L. Tsisun, B.K. Nefedov, E.S. Shpiro, G.V. Antoshin, K.M. Minachev, React. Kinet. Catal. Lett. 24 (1984) 37.
[59] J.P. Holgado, R. Alvarez, G. Munuera, Appl. Surf. Sci. 161 (2000) 301.
[60] S. Sharma, M.S. Hegde, J. Chem. Phys. 130 (2009) 114706.
[61] H. Cordatos, T. Bunluesin, J. Stubenrauch, J.M. Vohs, R.J. Gorte, J. Phys. Chem. 100 (1996) 785.
[62] R.J. Gorte, AIChE J. 56 (2010) 1126.
[63] G. Zhou, P.R. Shah, T. Montini, P. Fornasiero, R.J. Gorte, Surf. Sci. 601 (2007) 2512.
[64] S. Kim, R. Merkle, J. Maier, Surf. Sci. 549 (2004) 196.
[65] Y.M. Chiang, E.B. Lavik, D.A. Blom, Nanostruct. Mater. 9 (1997) 633.
[66] K. Zhou, X. Wang, X. Sun, Q. Peng, Y. Li, J. Catal. 229 (2005) 206.
[67] E. Mamontov, T. Egami, R. Brezny, M. Koranne, S. Tyagi, J. Phys. Chem. B 104 (2000) 11110.
[68] C. Adachi, T. Masui (Eds.), Synthesis and Modification of Ceria-based Materials, Imperial College Press, London, 2002.
[69] V. Perrichon, A. Laachir, G. Bergeret, R. Frety, L. Tournayan, O. Touret, J. Chem. Soc. Faraday Trans. 90 (1994) 773.
[70] A. Laachir, V. Perrichon, A. Badri, J. Lamotte, E. Catherine, J.C. Lavalley, J. El Fallah, L. Hilaire, F. Le Normand, E. Quemere, G.N. Sauvion, O. Touret, J. Chem. Soc. Faraday Trans. 87 (1991) 1601.
[71] C. de Leitenburg, A. Trovarelli, J. Kaspar, J. Catal. 166 (1997) 98.
[72] F. Giordano, A. Trovarelli, C. de Leitenburg, M. Giona, J. Catal. 193 (2000) 273.
[73] K. Otsuka, Y. Wang, E. Sunada, I. Yamanaka, J. Catal. 175 (1998) 152.
[74] S. Bernal, J.J. Calvino, G.A. Cifredo, J.M. Gatica, J.A.P. Omil, J.M. Pintado, J. Chem. Soc. Faraday Trans. 89 (1993) 3499.
[75] E. Aneggi, J. Llorca, M. Boaro, A. Trovarelli, J. Catal. 234 (2005) 88.
[76] S. Bernal, G. Blanco, J.M. Gatica, J.A. Perez-Omil, J.M. Pintado, H. Vidal, in: G. Adachi, N. Imanak, Z.C. Kang (Eds.), Binary Rare Earth Oxides, Dordrecht, Netherlands, 2004.
[77] C. Li, Y. Sakata, T. Arai, K. Domen, K.-i. Maruya, T. Onishi, J. Chem. Soc. Faraday Trans. 1: Phys. Chem. Condens Phases 85 (1989) 929.
[78] C. Li, Y. Sakata, T. Arai, K. Domen, K. Maruya, T. Onishi, Chem. Commun. (1991) 410.
[79] G. Marbán, I. López, T. Valdés-Solís, Appl. Catal. A: Gen. 361 (2009) 160.
[80] O. Pozdnyakova, D. Teschner, A. Wootsch, J. Kröhnert, B. Steinhauer, H. Sauer, L. Toth, F.C. Jentoft, A. Knop-Gericke, Z. Paál, R. Schlögl, J. Catal. 237 (2006) 1.
[81] O. Pozdnyakova, D. Teschner, A. Wootsch, J. Kröhnert, B. Steinhauer, H. Sauer, L. Toth, F.C. Jentoft, A. Knop-Gericke, Z. Paál, R. Schlögl, J. Catal. 237 (2006) 17.
[82] T. Shido, Y. Iwasawa, J. Catal. 141 (1993) 71.
[83] C. Binet, M. Daturi, J.-C. Lavalley, Catal. Today 50 (1999) 207.
[84] S. Chrétien, H. Metiu, Catal. Lett. 107 (2006) 143.
[85] V. Shapovalov, H. Metiu, J. Catal. 245 (2007) 205.
[86] R.G.S. Pala, H. Metiu, J. Phys. Chem. C 111 (2007) 8617.
[87] R.G.S. Pala, H. Metiu, J. Catal. 254 (2008) 325.
[88] M. Nolan, V. Soto Verdugo, H. Metiu, Surf. Sci. 602 (2008) 2734.
[89] H.Y. Kim, H.M. Lee, R.G.S. Pala, V. Shapovalov, H. Metiu, J. Phys. Chem. C 112 (2008) 12398.
[90] B. Li, H. Metiu, J. Phys. Chem. C 114 (2010) 12234.
[91] R.G.S. Pala, W. Tang, M.M. Sushchikh, J.-N. Park, A.J. Forman, G. Wu, A. Kleiman-Shwarsctein, J. Zhang, E.W. McFarland, H. Metiu, J. Catal. 266 (2009) 50.
[92] M.V. Ganduglia-Pirovano, J.L.F. Da Silva, J. Sauer, Phys. Rev. Lett. 102 (2009) 026101.
[93] H. Metiu, Physical Chemistry: Thermodynamics, Taylor and Francis Group, New York, 2006.
[94] U. Scherz, M. Scheffler, Semicond. Semimetals 38 (1993) 1.
[95] A. Franciosi, C.G. Van de Walle, Surf. Sci. Rep. 25 (1996) 1.
[96] C.G. Van de Walle, J. Neugebauer, J. Appl. Phys. 95 (2004) 3851.
[97] W. Kohn, in: F. Seitz, D. Turnbull (Eds.), Solid State Physics: Advances in Research and Applications, Academic Press, New York, 1957.